Iron-Sensitized Solar Cells (FeSSCs)

Mariachiara Pastore, Stefano Caramori, Philippe Gros

Iron-sensitized solar cells (FeSSCs)

Mariachiara Pastore,[a] Stefano Caramori,[b] and Philippe C. Gros ,[c]*

a) Université de Lorraine, CNRS, LPCT, F-54000 Nancy. b) Department of Chemical and Pharmaceutical Sciences, University of Ferrara,Via L.Borsari 46, 44121, Ferrara, Italy. c) Université de Lorraine, CNRS, L2CM, F-54000 Nancy

*E-mail : philippe.gros@univ-lorraine.fr

Conspectus

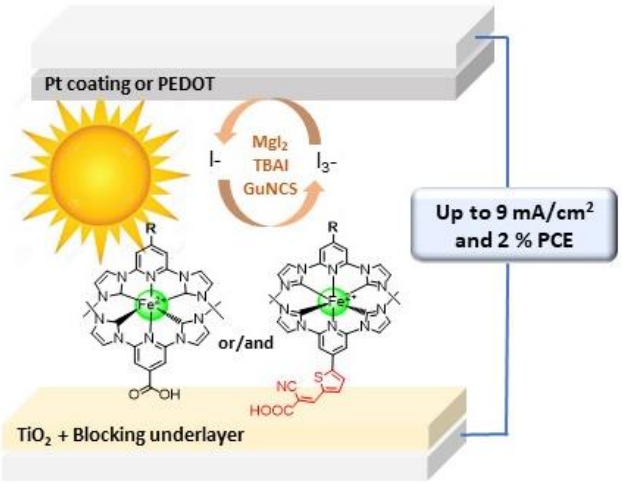

The harvesting and conversion of solar energy has become a burning issue for our modern societies seeking to move away from the exploitation of fossil fuels. In this context, Dye-sensitized solar cells (DSSCs) have proved to be trustworthy alternatives to silicon-based cells with advantages in terms of transparency and efficiency under low illumination conditions. These devices are highly dependent on the ability of the sensitizer that they contain to collect sunlight and transfer an electron to a semiconductor after excitation. Ruthenium and polypyridine complexes are benchmarks in this field, as they exhibit ideal characteristics such as long-lasting metal-ligand charge transfer (MLCT) states and efficient

separation between electrons and holes, limiting recombination at the dye-semiconductor interface. Despite all these advantages, ruthenium is a noble metal, and the development of more sustainable energy devices based on earth-abundant metals is now a must. A quick glance at the periodic table reveals iron as a potential good candidate, since it is in the same column as ruthenium that suggests similar electronic properties. However, striking photophysical differences exist between ruthenium(II) polypyridyl complexes and their Fe(II) analogues, the latter suffering from short-lived MLCT states resulting of their ultra-fast relaxation into metal-centered (MC) states. Pyridyl-N-heterocyclic carbenes (pyridylNHC) brought a strong σ-donor character required to promote a higher ligand field splitting of the iron d orbitals, resulting in a destabilization of the MC states over the MLCT manifold with slowdown of the excited state deactivation providing iron(II) complexes with tens of picoseconds lifetimes making them more promising for applications in DSSCs. This account highlights our recent advances in the development and characterization of iron-sensitized solar cells (FeSSCs) with a focus on the design of efficient sensitizers going from homoleptic to heteroleptic complexes (bearing different anchoring groups) and on electrolyte contents. Our rational approach led to the best photocurrent and efficiency ever reported for an iron sensitized solar cell (2% PCE and 9 mA/cm^2) using a co-sensitization process. These works clearly evidence that the solar energy conversion area based on iron complexes sensitization is now opened.

Key references

- Duchanois, T.; Etienne, T.; Cebrián, C.; Liu, L.; Monari, A.; Beley, M.; Assfeld, X.; Haacke, S.; Gros, P. C. An Iron-Based Photosensitizer with Extended Excited-State Lifetime: Photophysical and Photovoltaic Properties: An Iron-Based Photosensitizer with Extended Excited-State Lifetime. *Eur. J. Inorg. Chem.* **2015**, *2015* (14), 2469–2477.[1]

This paper was the very first proof-of-concept of an FeNHC-sensitized DSSC using a dicarboxylic homoleptic iron complex.

- Reddy Marri, A.; Marchini, E.; Diez Cabanes, V.; Argazzi, R.; Pastore, M. ; Caramori, S. ; Gros, P.C. Record power conversion efficiencies for Iron (II)-NHC-sensitized DSSCs from rational molecular engineering and electrolyte optimization *J. Mater. Chem. A,* **2021**, 9, 3540-3554.[2]

  In this paper, we investigated a series of new heteroleptic complexes (mono carboxylic) and improved the photocurrent significantly by combining them with a newly designed electrolyte.

- Reddy Marri, A.; Marchini, E. ; Diez Cabanes, V. ; Argazzi, R.; Pastore, M. ; Caramori, S. ; Bignozzi, C.A.; Gros, P.C., A series of Iron(II)-NHC Sensitizers with record power conversion efficiency in photoelectrochemical cells, *Chem. Eur. J.*, **2021**, 27, 16260–16269.[3]

  We have demonstrated that the electronic properties of the Fe sensitizer could be deeply modified by substitution on the ligand not attached to the semiconductor and favour charge separation by push-pull effects. This boosted both the photocurrent and efficiency.

- Reddy-Marri, A.; Marchini, E.; Cabanes, V. D.; Argazzi, R.; Pastore, M.; Caramori, S.; Gros, P. C. Panchromatic Light Harvesting and Record Power Conversion Efficiency for Carboxylic/Cyanoacrylic Fe(II) NHC Co-Sensitized FeSSCs. *Chem. Sci.* **2023**, *14* (16), 4288–4301.[4]

  The co-sensitization of the semiconductor using two different iron complexes one of them bearing cyano acrylic moieties has been investigated. It produced a panchromatic absorption and photocurrent improvement up to 9 mA.cm^{-2} never obtained for a Fe-sensitized DSSC.

Introduction

Nowadays, dye-sensitized solar cells (DSSCs) have reached a mature technology level, representing a valuable opportunity to build solar cells highly modulable in shape, transparency and color.[5] Moreover, a peculiar merit of DSSCs is the possibility of being efficiently employed in indoor conditions,[6,7] paving the way to their use as power sources in Internet of Things (IoT) devices and wireless network sensors in ambient environments.[8]

DSSC functioning mechanism, schematized in Figure 1a), mimics the way nature absorbs energy from the sun: a semiconductor (SC, generally TiO_2) sensitized with a dye is, indeed, at the core of this photovoltaic technology.[9]

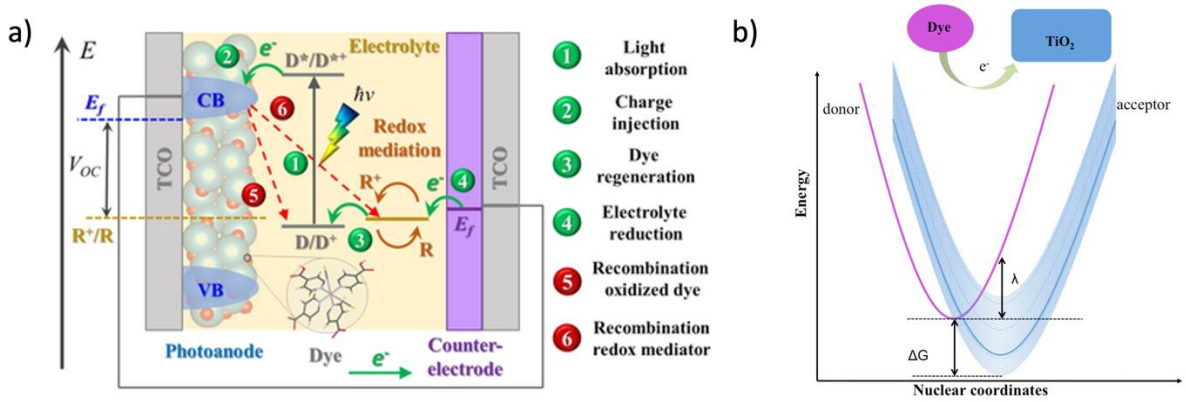

Figure 1. a) Operating scheme of a DSSC. Continuous green/orange arrows are used to indicate the desired electron transfer processes, whereas dashed red lines indicate parasitic recombination processes; Adapted with permission from ref.[10]. Copyright 2023 Elsevier. **b)** Energetics of the electron transfer between a donor (left side) and a quasi-continuum of acceptor states (right side) typical of dye/SC interfaces. Adapted with permission from ref.[11]. Copyright 2013 Springer Nature.

Upon solar light absorption (1), the sensitizer injects the photoexcited electron into the SC's conduction band (2). A redox mediator (generally the I_3^-/I^- couple in an electrolyte) then regenerates the ground state of the sensitizer (3) and is finally restored at the cathode, closing the electrical circuit (4).

The cell efficiency is defined as:

$$\eta = \frac{V_{oc} J_{sc} FF}{PI} \quad (1)$$

where V_{oc} (the open circuit voltage) is the difference between the quasi-Fermi level (E_f) of TiO_2 under illumination and the redox potential of the redox couple (R^+/R), J_{SC} is the short circuit photocurrent density, FF is the fill factor and PI is the intensity of the incident light. J_{SC} is defined as integral over the solar spectrum of the monochromatic incident photon to current conversion efficiency (IPCE) under short circuit conditions:

$$IPCE=LHE \times \phi_{inj} \times \phi_{COLL} \qquad (2)$$

where LHE is the light harvesting efficiency of the photoelectrode, ϕ_{inj} the quantum yield of electron injection and ϕ_{COLL} the electron collection efficiency at the TCO. From a phenomenological point of view, the quantum efficiency for charge injection ϕ_{inj} is given by the ratio between the electron transfer rate constant (k_{inj}) and the sum of all the rate constants causing deactivation of the excited state.

$$\phi_{inj} = \frac{k_{inj}}{\sum_i^n k_i} \quad (3)$$

The probability of electron transfer involving the excited state of the sensitizer and the acceptor states in the semiconductor (Figure 1b)) can be treated non-adiabatic radiationless process[12] in the framework of the Fermi's "Golden Rule":

$$k_{inj} = \frac{2\pi}{\hbar}\mathcal{V}_{if}^2\rho(E_f)_{Ef\approx Ei} \quad (4)$$

Where k_{inj} is rate constant of the transition from the initial state (i) to the final state (f), depending on the product of the squared matrix element *Vif* with the density of final states (charge separated states) isoergonic with the initial states. $\mathcal{V}_{if} = \langle\psi_i|H|\psi_f\rangle$ where ψ_i and

ψ_f are the wavefunctions of the initial and final state and H represent the perturbation Hamiltonian that promotes the transition (i.e. non adiabatic coupling operators).[13] Thus, the probability of electron transfer k_{inj} depends both on the energetic (through $\rho(E_f)$) and spatial overlaps (through $\mathcal{V}_{if}$) of the initial and final states involved in the transition (see Figure 1b)). It is clear from (3) that $\phi_{inj} \to 1$ only if $k_{inj} \approx \sum_i^n k_i$, or, in other words, k_{inj} should be at least one order of magnitude larger than the sum of the other wasteful deactivation rate constants. Thus, it is clear from equations (3) and (4) that a rational design of an efficient sensitizer should try to optimize the energetic and spatial properties of the excited state for a fast charge injection, and, at the same time, increase the excited state lifetime (i.e. decrease as much as possible the k_i competing with k_{inj}.)

In the last decades, the development of new materials to increase the devices' stability and optimize the photovoltaic performances, has represented the main focus of the scientific and technological research.[14–17] In the last years, increasing efforts addressed the sustainability and greenness of the developed materials applying a holistic approach.[18–21] Historically, ruthenium-based sensitizers are the gold standard,[22,23] having reached the highest certified efficiency for DSSCs (12.3%). This leadership has been achieved thanks to exceptional properties of these sensitizers[24–27] combining long-lived MLCT states from which the electron is transferred into the semiconductor conduction band (CB) and efficient electron-hole separation thus limiting the back-recombination processes.[28–30]

Nonetheless, ruthenium has been included in the list of critical raw materials (CRMs) by the EU, thus, hampering any potential future large-scale application.

The attention has been thus focused on alternative sensitizers such as earth abundant transition metal complexes[31,32] or metal-free conjugated compounds.[33–35] The first iron-based sensitizer was reported by Ferrere[36,37] using *cis*-Fe^{II}(2,2′-bipyridine-4,4′dicarboxylic acid)$(CN)_2$ with albeit a very poor photoconversion efficiency. This fate is a consequence of the short-lived MLCT states of Fe(II) polypyridine complexes resulting of an ultrafast (fs regime) relaxation to metal centered (MC) states and subsequent ground-state recovery.[38–43] The advent of N-heterocyclic carbenes (NHC) as strong field ligands has sparked the revival of the quest for iron complexes with long-lived MLCTs resulting in a destabilization of the MC states over the MLCT manifold with slowdown of the excited state deactivation (Figure 2).[44–50]

Indeed, besides DSSCs, the development of a photochemically stable class of first row metal complexes with long lived excited or charge separated states holds out the hope of widespread applications in photocatalysis and in the emerging field of photoredox chemistry.[51,52]

This strategy has paved the way for the preparation of iron(II) complexes with MLCT state lifetimes of tens of picoseconds, giving more credit for their potential application in DSSCs. Despite the remarkable progresses in the lifetimes of iron(II) MLCT states, however, fabrication of efficient DSSCs devices has proved to be challenging, with reported record efficiency of about 2%[4] that are still far from those reported for ruthenium(II) dyes. However, this field is still at its infancy, and there are still many options to improve the overall efficiency by exploring the use of different redox shuttles and optimizing the semiconductor electrodes.

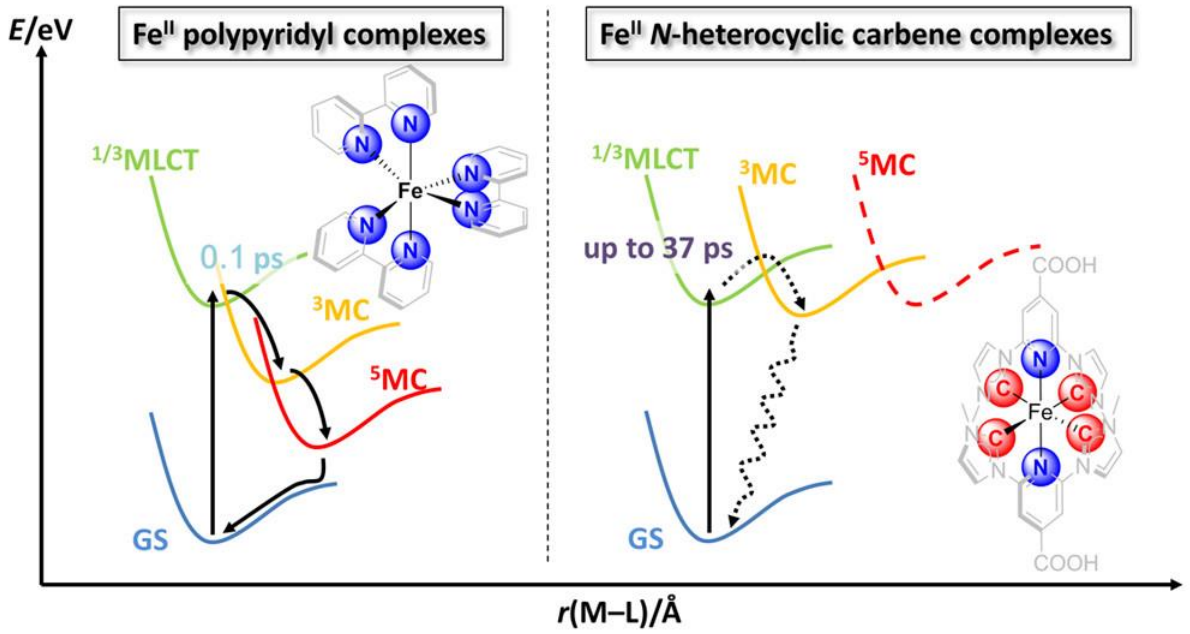

Figure 2. Energetic landscapes of a Fe(II) polypyridine complex (left) and Fe(II) pyridylNHC complex **C1** (right). Reprinted with permission from ref.[46]. Copyright @ 2016 American Chemical Society

This account highlights the recent advances in the development of iron-sensitized solar cells (FeSSCs), that are essentially based on two different strategies: the chemical engineering of the dye[3,4,53–56] and the optimization of the electrolyte composition.[2,57–59] The impact of the sensitizer design, the electrolyte contents as well as the energetics and charge transfer processes at play in iron FeSSCs will be discussed on the basis of photoelectrochemical, photophysical and computational investigations.

Photoelectrochemical investigations with a prototypal homoleptic sensitizer

The prototypal sensitizer first investigated was complex **C1** (Figure 2, right)[1,60] where the iron center is coordinated to two pyridyl(NHC)$_2$ ligands, where both ligands have been equipped with a carboxylic function required for the chemisorption on TiO_2 surface and to ensure the electronic transfer. The four NHC ligands surrounding the metal combined to the electron-withdrawing

COOH on the central pyridine promoted an unprecedented increase of the MLCT lifetime up to 18 ps.[1,60] Warnmark et al have performed ultrafast time-resolved THz spectroscopy analysis on a separate **C1**-sensitized TiO_2 photoanode (in the absence of any other DSSC components) that revealed that the interfacial injection should promisingly occur with 92% yield.[60]

We have assembled the first DSSCs using **C1** as a sensitizer and their photoelectrochemical properties were investigated (Table 1 and Figure 3) and rationalized based on the results of theoretical calculations.[2,53] The SC was a commercial transparent TiO_2 (20 nm nanoparticles, Greatcell Solar 18NR-T) made with (*BUL*) and without (*no BUL*) a blocking underlayer obtained by first spin coating 0.3 M $Ti(OiPr)_4$ (0.3 M) on the FTO (conducting glass). A range of electrolytes was tested, including Solaronix Iodolyte AN50 (that contains *t*BuPyridine as basic additive to improve the open circuit voltage of the cell)[61] and a base-free formulation consisting in LiI (0.1 M), I_2 (0.1 M), PMII (1-methyl-3-propyl-imidazolium iodide, 0.6 M) in acetonitrile. This formulation was modified by addition of either MgI_2 (0.05 M) (*el*1) or MgI_2 (0.1 M) + GuNCS (Guanidinium thiocyanate, 0.1 M) (*el*2) or MgI_2 (0.1 M) + GuNCS (0.1 M) + TBAI (tetrabutylammonium iodide, 0.1 M) (*el*3*)*

Table 1. Efficiency parameters from **C1**-sensitized DSSCs containing various electrolytes with or without a Blocking underlayer (BUL).

BUL	electrolyte	*J*sc/(mA.cm^{-2})	*V*oc (V)	*FF*	PCE%
no	iodolyte AN50	0.41	0.46	0.68	0.13
no	*el*1	2.34	0.38	0.55	0.49
yes	*el*1	3.34	0.38	0.59	0.75
yes	*el*2	3.30	0.44	0.63	0.92

At first, Iodolyte AN50, an electrolyte optimized for ruthenium dyes like N719, led to a very poor efficiency,[1] that has been traced back to fast recombination dynamics with the electrolyte,[36] and to an inappropriate direction of the charge flow in the lowest MLCT states of the homoleptic compound, impeding electron injection.[53] DFT calculations of **C1**@TiO_2 electronic structure and electron injection kinetics revealed that the lowest-energy MLCT state indeed promotes charge transfer from the metal to the not-anchored NHC ligand, thus quenching the electron injection (see the LUMO/LUMO+1 localization in the top of Figure 4).

Switching to *el1* and its Mg^{2+}content significantly improved both the photocurrent and the efficiency. The blocking underlayer (*BUL*) expected to prevent recombination of photoinjected electrons with I_3^-, promoted a notable improvement in photovoltaic efficiency (from 0.49 to 0.75 %). *el2*, containing GuNCS and MgI_2 (0.1M) led to an unprecedented performance for a Fe(II) sensitizer, with J_{sc}=3.3 mA/cm^2, Voc = 0.44 V, *FF*=0.63 and PCE≈1%.[62] GuNCS slightly enhanced the fill factor and Voc, signing an effect on recombination inhibition, while Mg^{2+}, a high charge density cation, capable to adsorb onto the TiO_2, enhanced the surface dipole for charge injection and brought a surface excess of I^-, thus accelerating dye regeneration.[63,64]

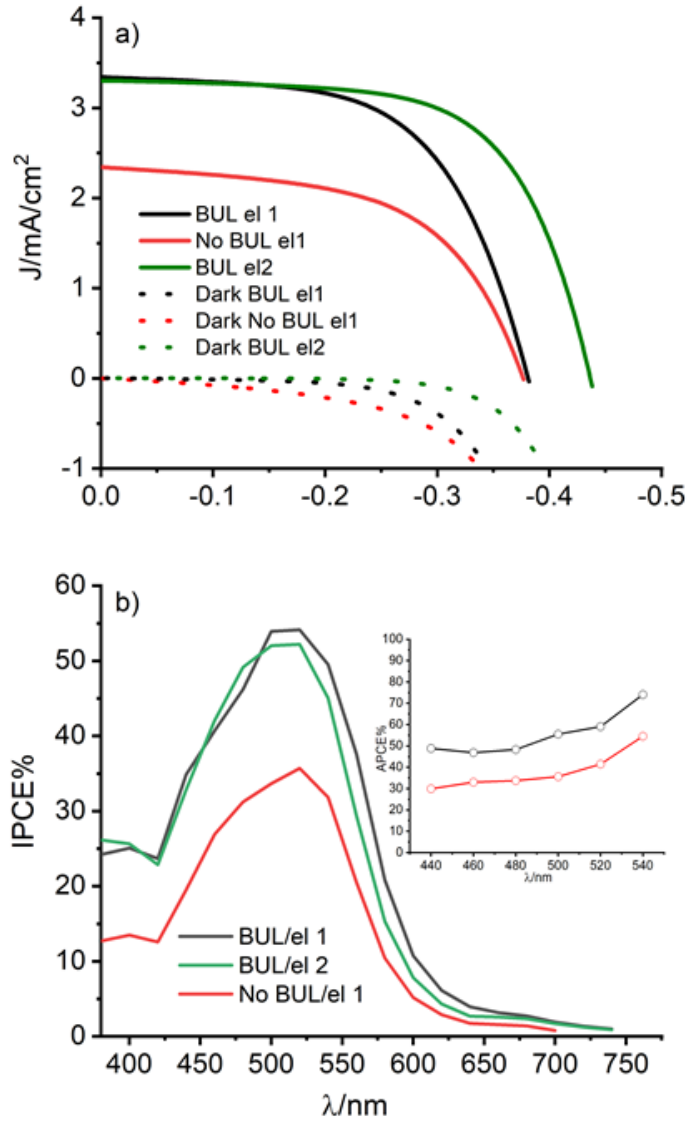

Figure 3. a) *J*/*V* curves of **C1** sensitized cells filled with *el*1 and *el*2 electrolytes under AM 1.5G illumination and in the dark (dotted lines). b) Photoaction spectra (IPCE vs λ) showing a maximum efficiency of ca. 50% in the best conditions. APCE (APCE=IPCE/LHE) in inset. Data from ref. [57]

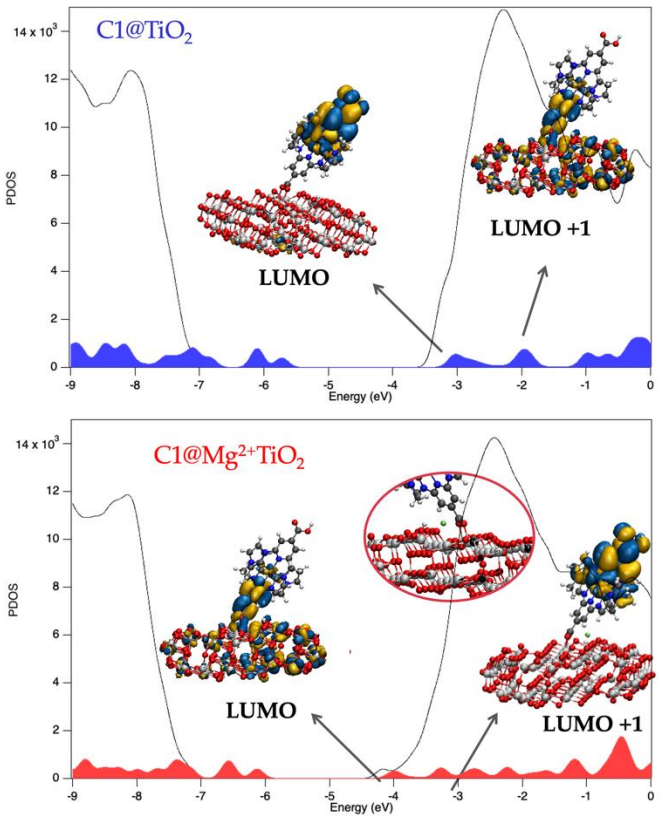

Figure 4. Calculated (B3LPY*/6-311G(d)//PCM(MeOH)) partial density of states (PDOS) for the **C1**@TiO_2 (top) and **C1**@$Mg^{2+}TiO_2$ (bottom) interface models. Filled red/blue profiles correspond to C1 PDOS while black lines plot the TiO_2 PDOS. The isosurface density plots of LUMO and LUMO+1 are also shown to represent the inversion of the charge transfer direction at the interface when Mg^{2+} cations are adsorbed. Data from ref. 2

The effect of the Mg^{2+} salts in the electrolyte on the photocurrent was rationalized by modelling the **C1**@$Mg^{2+}TiO_2$ interface (bottom panel in Figure 4). Localizing the positive charge close to the anchoring unit stabilizes the CT toward the surface-adsorbed ligand allowing the lowest-energy MLCT transition to recover the appropriate directionality thus promoting an ultrafast electron transfer.

Housecroft and coworkers have studied in detail the impact of imidazolium salts' nature and their associated anions in electrolytes (in the absence of Mg^{2+}) on cell efficiency. Using **C1** as the sensitizer, the efficiencies never exceeded the 0.5-0.6% range.[65]

We have examined the charge transfer dynamics state using transient absorption spectroscopy (TAS) in the ns-ms time scale, in order to investigate the recombination and regeneration kinetics relevant for the operation of the DSSC (Figure 5). Figure 5b shows that the photoinjection from **C1** into TiO_2 is almost instantaneous for the instrumental response of the spectrometer, (FWHM 7 ns), producing a long lived charge separated state ($e^-(TiO_2)$/Fe(III)), having as a main spectral fingerprint, the bleaching of the 510 nm MLCT band surviving hundreds of milliseconds. Photogenerated Fe(III) could be reconverted to Fe(II) with a nearly unitary efficiency by I^- at the concentration used for the photoelectrochemical measurements of Figure 3, showing that the competition between recombination and regeneration is not critical with the optimized electrolytes (Figure 5a). However, the TAS spectra at early delays (0-4 ns) revealed a narrowing and blue shifting of the ground state bleaching band concomitant to the disappearance of a weak absorption band in the lower energy region ($\lambda > 650$ nm). These features were assigned to the relaxation of a residual population of the lowest triplet state (T1) unable to inject, consistent with the APCE $\approx$ 50% in the best conditions of Figure 3b and indicating the persistence of a less than optimal kinetic competition between electron transfer and non-radiative excited state decay.

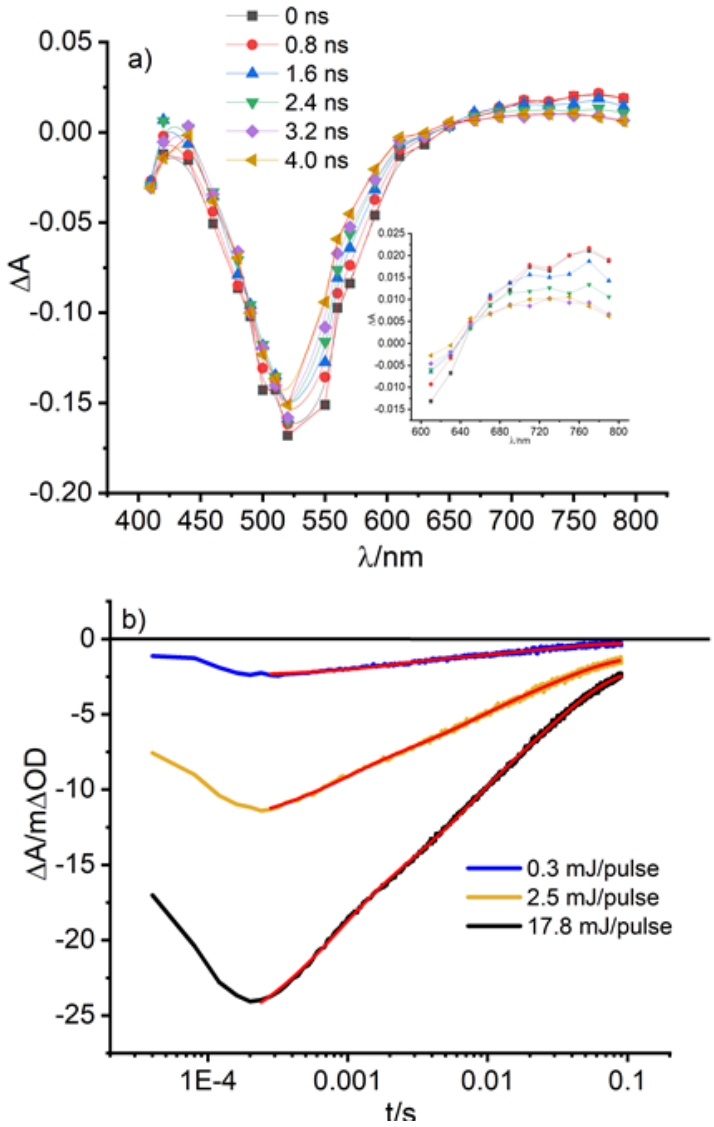

Figure 5. a) TAS of **C1** chemisorbed on TiO_2 in contact with $LiClO_4$ (0.1M) in ACN (532 nm excitation) at short delays (4 ns) after the laser pulse; b) Charge recombination kinetics in **C1**@TiO_2 photoanodes at 500 nm measured under different excitation energies. Data from ref. [57]

Impact of dissymmetry in sensitizers

As discussed above, the pioneering work of the prototypal **C1** revealed an incomplete electron injection, resulting from a charge transfer vs excited state's deactivation kinetic competition that originate from a non-optimal electronic coupling due to lack of directionality of the MLCT excited state, arising from the symmetric design of **C1**.[53] We have therefore focused on the

synthesis of a collection of sensitizers based on heteroleptic complexes deprived of one of the COOH groups and enabling electronic modulations by decorating the 4 position released on the central pyridine (Figure 6).[2,3] All these heteroleptic complexes have been prepared according to the statistical approach that we have developed (Scheme 1). Along the same line, the group of Warnmark also prepared push-pull complexes **C2** and **C3** bearing diphenylamino groups.[54] (Figure 6).

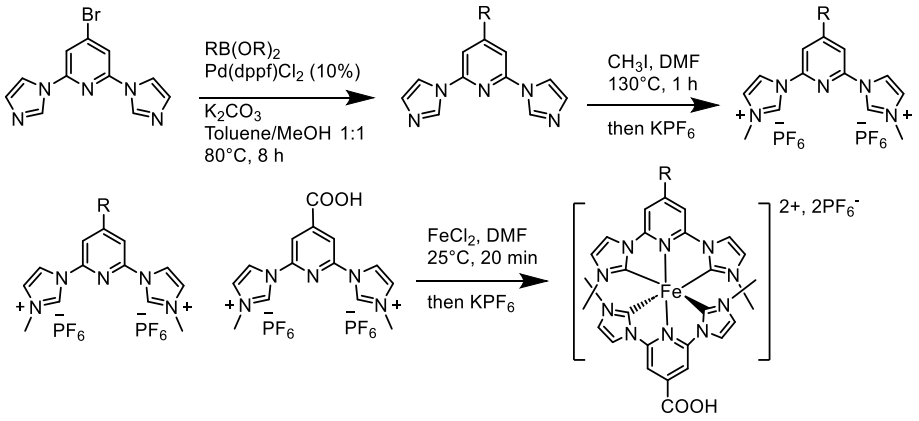

Scheme 1. General synthetic route to ligand precursors and heteroleptic complexes of Figure 6.

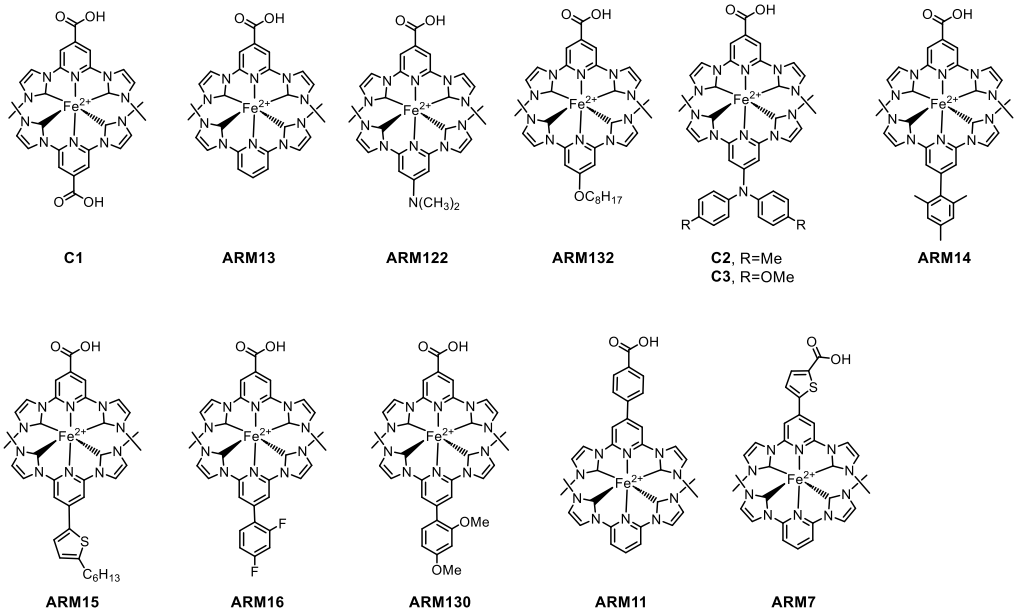

Figure 6. Chemical structures of heteroleptic complexes and of prototypal complex **C1**

The efficiency parameters obtained from DSSC sensitized with complexes of Figure 6 are collected in Table 2. In each case the photoanode/cathode characteristics and the electrolytes used are indicated.

The results obtained with **ARM13**, **ARM11** and **ARM7** revealed that the introduction of an aromatic spacer between the complex and the COOH group, intended to suppress the spatial overlap between the injected electron and Fe(III), and thus slow down recombination, was found deleterious for the photocurrent, despite the increased optical absorption, also pointing to the fact that injection rather than recombination is a limiting factor with this design of Fe(II) sensitizers.[2] This was explained by the relative percentages of electron density localized on the anchoring COOH: respectively 16.3%, 8.3 % and 6.7% for **ARM13**, **ARM7** and **ARM11**(Figure 7). These values were directly correlated with the photocurrents of 3.95 (**ARM13**), 3.55 (**ARM7**) and 2.69 mA/cm^2 (**ARM11**) reported in Table 2.

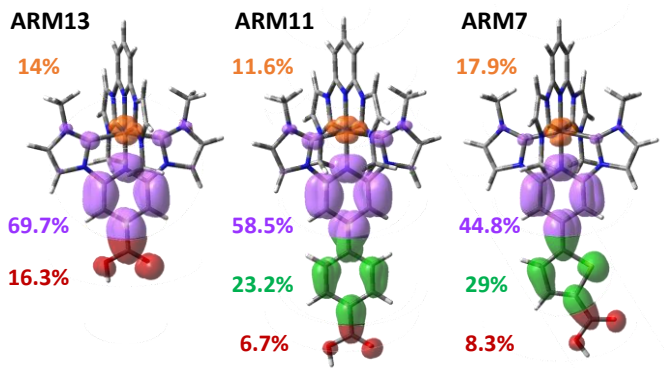

Figure 7. Electron Natural Transition Orbitals (NTOs) in **ARM13**, **ARM11** and **ARM7** with the percentages of delocalization. Data from ref. 2

Table 2: Cell efficiency parameters from **Fe(II)NHC** (Figure 6)-sensitized solar cells using different photoanodes and cathodes as well as various electrolytes contents.

Sensitizer	Electrolyte	*J*sc (mA/cm^2)	*V*oc(V)	FF (%)	PCE (%)	reference
N719[a,c]	*el2*	12.84	0.48	58	3.57	[2]
C1 [a,c]	*el2*	3.64	0.45	62	1.02	[2]
C1[b,c]	*el2*	4.02	0.51	59	1.14	[2]
C1[a,d]	*el3*	5.60	0.44	56	1.39	[3]
C1[e,f]	*el4*	2.09	0.47	75	0.63	[54]
ARM7[a,c]	*el2*	3.55	0.44	60	0.94	[2]
ARM11 [a,c]	*el2*	2.69	0.46	63	0.78	[2]
ARM13 [a,c]	*el2*	3.95	0.49	61	1.18	[2]
ARM13 [a,c]	*el3*	4.44	0.45	64	1.27	[2]
ARM13[b,c]	*el2*	4.26	0.51	59	1.29	[2]
ARM13[b,c]	*el3*	4.98	0.47	62	1.44	[2]
ARM16 [a,c]	*el3*	4.87	0.43	59	1.24	[3]
ARM122 [a,c]	*el3*	4.82	0.37	51	0.91	[3]
ARM130 [a,c]	*el3*	5.59	0.44	58	1.43	[3]
ARM122 [a,d]	*el3*	6.11	0.39	49	1.17	[3]
ARM130 [a,d]	*el3*	6.80	0.47	57	1.83	[3]
ARM14 [a,d]	*el3*	6.03	0.47	59	1.68	[3]
ARM15 [a,d]	*el3*	6.07	0.43	61	1.58	[3]
ARM16 [a,d]	*el3*	5.81	0.47	57	1.56	[3]
ARM132 [a,d]	*el3*	5.20	0.35	61	1.11	[3]
C2 [e,f]	*el4*	3.52	0.51	72	1.2	[54]
C3 [e,f]	*el4*	3.23	0.42	69	0.8	[54]

[a] PEDOT cathode was used. [b] Reflective platinum coated cathode. [c] 16 μm TiO_2. [d] 20 μm TiO_2 + scattering layer. [e] *el4* = LiI (0.1M), I_2 (0.05M) and 1,2-dimethyl-3-propylimidazolium iodide (0.6 M) in 3-methoxypropionitrile. [f] 32 μm TiO_2 + scattering layer

Among **ARM13**, **ARM11** and **ARM7**, the best PCE was recorded for **ARM13** (1.18%) offering the best photocurrent (3.95 mA/cm^2), photovoltage (0.49 V) and FF (61 %). Notably **ARM13** displayed the lowest dark current in agreement with the best Voc obtained in this series (Figure 8).

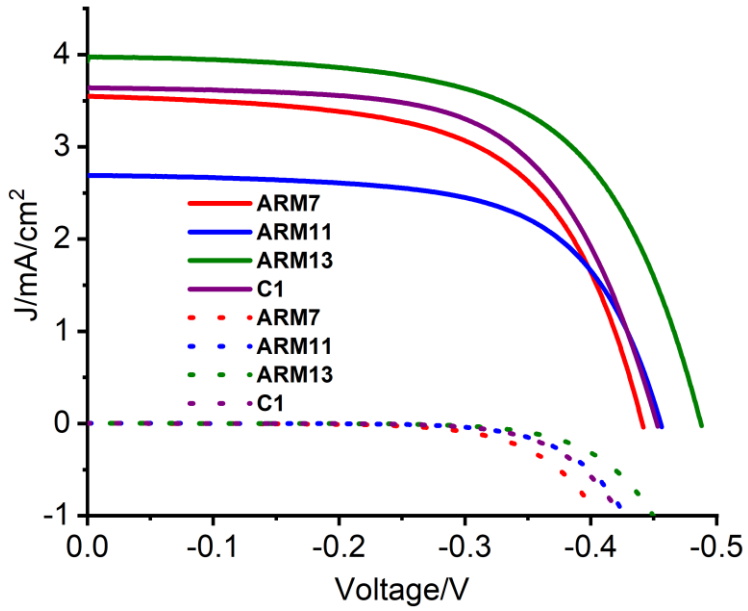

Figure 8. *J*/*V* curves obtained with *el2* under AM 1.5G illumination (solid lines) and in the dark (dotted lines). Data from ref.2

Notably the computed interfacial electron injection kinetics agreed with the photocurrents measured for **C1** and **ARM13**, indicating a slightly higher electronic coupling (0.179 vs. 0167 eV) for **ARM13**, despite its weaker light harvesting capability.[2]

The effect of substituents on the pyridine ring has been investigated first on **ARM122** bearing a donating dimethylamino group, **ARM16** decorated with an electron withdrawing difluorophenyl group and **ARM130** with its donating dimethoxyphenyl group. When **ARM16**, **ARM122** and **ARM130** were chemisorbed on a 16 µm TiO_2 and *el*3 was used. 1.43 %. 1.24 %, and 0.91 % PCE were obtained for **ARM130**, **ARM16**, and **ARM122** respectively. A scattering

top layer was then applied to better collect light at longer wavelengths that are poorly absorbed by our sensitizers.[3]

Thanks to this top ayer, all the sensitizers performed better, **ARM130** being the best in the series with a *J*sc of 6.33 mA/cm^2, a *V*oc of 0.46 V and a PCE of 1.65%. Thickening the transparent active TiO_2 layer to ca. 20 µm (the light scattering overlayer was maintained) extended slightly the photoconversion threshold beyond 700 nm with the best photoconversion observed in the 450-650 nm range in agreement with the MLCT absorption of the sensitizers (Figure 9a). The *J*/*V* curves (Figure 9b) were in line with the action spectra, **ARM130** showing the best combination of *J*sc (ca. 7 mA/cm2) and *V*oc (0.47V) leading to a PCE of 1.83%. The sensitizers bearing an aromatic group as substituents gave much better efficiencies that those directly substituted by an heteroarom i.e. **ARM122** and **ARM132** (PCE% = 1.17 and 1.11 respectively). The push-pull sensitizers **C2** and **C3** decorated with diarylamino groups reported by Warnmark and chemisorbed on a 32 mm TiO_2 + scattering layer led to almost the same efficiency as **ARM122** with albeit a ca half value for the photocurrent.[54] Note that the electrolyte used here did not contain Mg^{2+}, GuSCN and TBAI.

Impact of the anchoring group

Since the anchoring group's interaction with the surface of the photoanode is critical to ensure an efficient injection and to prevent back recombination processes, the effect of the anchoring functionality has been investigated.[33] We have introduced the thienylcyanoacrylic moiety (ThCA) as anchoring group[66,67] that has been reported to exhibit a robust S…CN bond leading to two intramolecular charge transfers that should enhance the electron transfer.[67] Thus ThCA has been introduced on the complexes following Scheme 2.[4]

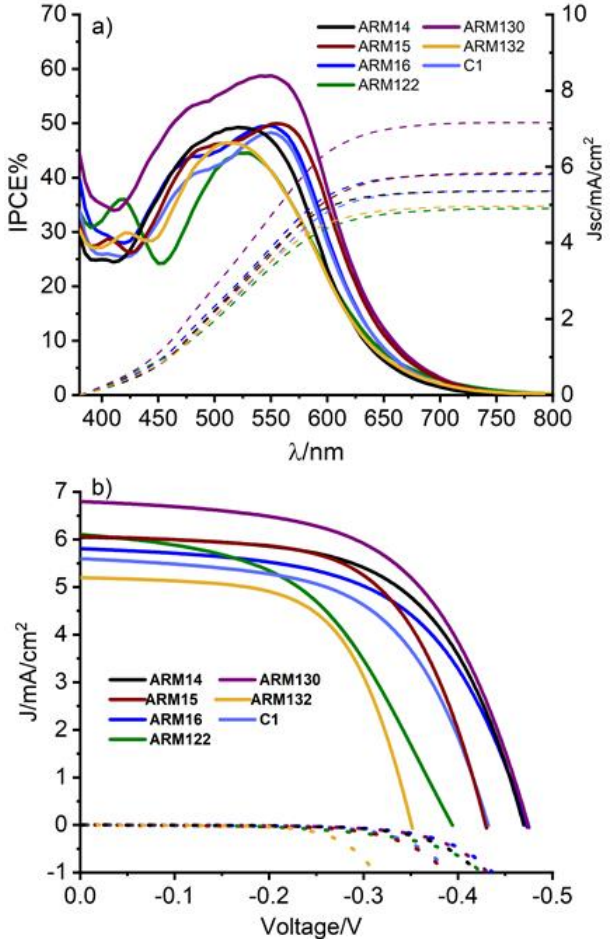

Figure 9. (a) IPCE spectra and the corresponding integrated photocurrent (dotted lines). (b) J/V curves under AM 1.5G illumination and in the dark (dotted lines) in the presence of *el*3. A photoanode ca. 20 μm thick TiO_2 plus a scattering layer were used. Data from ref. 4

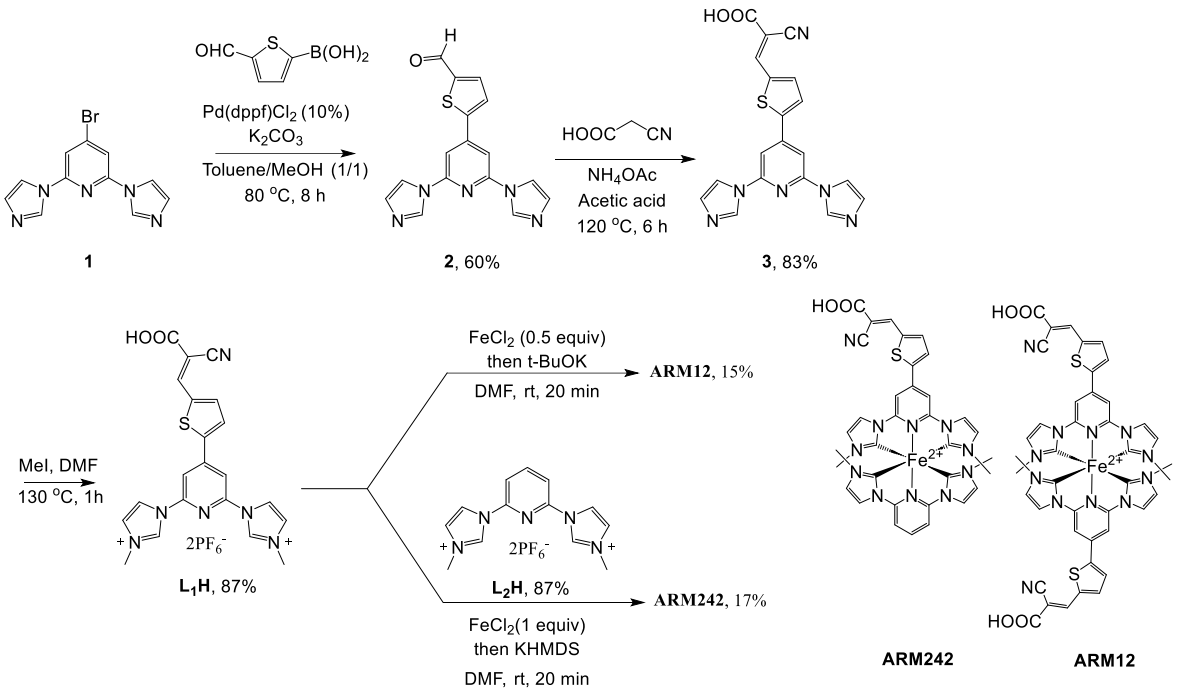

Scheme 2. Synthesis of ligand precursors and complexes **ARM12** and **AM242**

The absorption spectra of **C1**, **ARM12** and **ARM242** chemisorbed on a 13μm TiO_2 anode showed a strong red-shift of the MLCT band with **ARM12** and **ARM242** that however leaves an almost transparent window between 400 and 500 nm, where, in contrast **C1** strongly absorbs. Thus, to further improve the spectral sensitivity of the photoanodes, we have performed the co-sensitization of **C1** and **ARM12** that resulted in a nice panchromatic absorption from 450 to 700 nm (Figure 10).[4] DSSCs have been assembled including these sensitizers. A 20 μm TiO_2 with a scattering top layer, PEDOT-based counter electrode and *el3* were used. The photovoltaic results are found in Table 3.

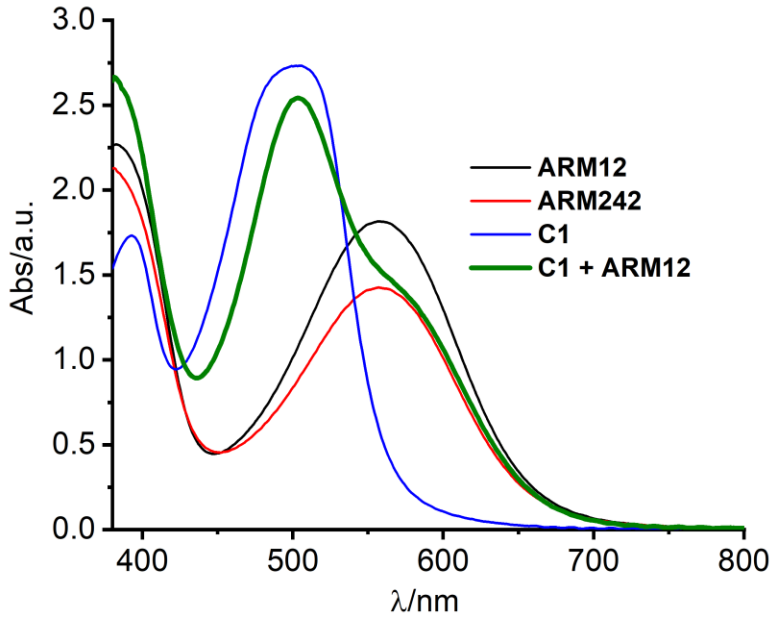

Figure 10. Absorption spectra (an identical dye-free electrode was used as a reference) of **C1** **ARM12**, **ARM242** and (**ARM12** + **C1)** loaded on 13 µm TiO_2. Data from ref. 4

Table 3: Cell efficiency parameters from thienocyanoacrylic based-**FeSSCs**

Sensitizer	Jsc (mA/cm^2)	Voc(V)	FF (%)	PCE (%)
ARM12	7.84	0.39	56	1.71
ARM242	6.64	0.39	59	1.52
C1	5.27	0.45	55	1.30
C1+ARM12	8.63 (8.74)[a]	0.42 (0.43)[a]	55 (55)[a]	1.98 (2.06)[a]

[a] Values reported in parentheses represent the parameters associated to the best cell.

The photocurrent current reached 7.84 mA/cm^2, 6.64 mA/cm^2 and 5.27 mA/cm^2 with a PCE of 1.71%, 1.52% and 1.30% for **ARM12, ARM242** and **C1** respectively (Figure 11a and Table 3).

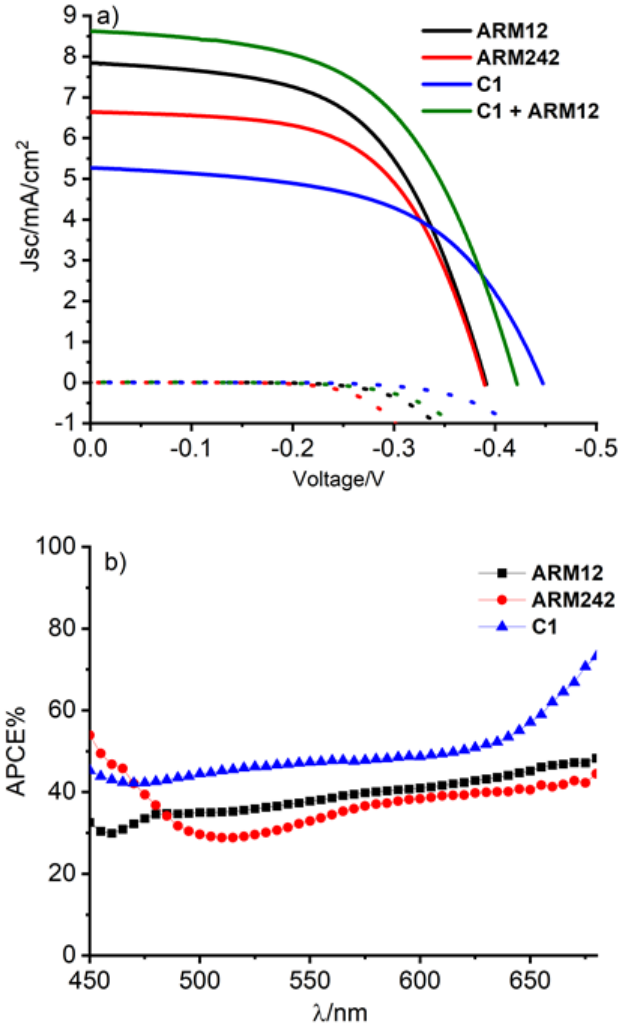

Figure 11. a) *J*/*V* curves for the Fe(II)NHC-sensitized TiO_2 electrodes (20 µm + scattering layer) under AM 1.5G illumination and in the dark (dotted lines). b) Absorbed Photon to Current Conversion Efficiency (APCE) spectra according to APCE=IPCE/LHE. Data from ref. 4

These photocurrent densities are the highest ever reported for an iron-based DSSC. The lower performances of **ARM242** compared to **ARM12** can result from both a slightly lower injection quantum yield (see APCE, Figure 11b) and a faster recombination with I_3^- signed by a less negative threshold of the dark current in Figure 11a.

Computing the electronic structure of the dye@TiO_2 interface and the electronic dye/metal oxide coupling allowed to rationalize the results and to quantify the impact of the ThCA anchoring

group on electron injection efficiency. As displayed in Figure 12a, the ThCA unit promoted a significant motion of the electron density from the Fe-NHC core towards the carboxylic group, inducing a larger electron delocalization around the anchoring moieties (almost 16% increase) for **ARM242** with respect to **ARM13.** Based solely on the optoelectronic properties of the standalone sensitizers (red-shifted absorption and higher electron localization on the anchoring group), higher photocurrents and higher PCEs for the ThCA-based dyes with respect to **ARM13**/**C1** could be expected. However, when chemisorbed on SC, the ThCA-based sensitizers were found strongly bent toward the surface, as a consequence of the extension of the π-conjugation increasing the Van der Waals interactions with the TiO_2 substrate. This particular configuration, breaking the electronic communication between the dye and the surface, weakens the LUMO-CB states electronic coupling, despite the larger fraction of charge localized upon excitation on the anchoring group (Figure 12a).

By calculating the electronic coupling of the dye's LUMO with the TiO_2 CB states, the electron injection probability (Γ_{inj}) over the semiconductor manifold of unoccupied levels was quantitatively estimated (Figure 12c). The Γ_{inj} values estimated for **ARM242,** regardless of the LUMO position (driving force)**,** are always lower with respect to the ones displayed by the COOH reference dye, indicating that the reduction in the electronic coupling due to the breaking of the dye-TiO_2 electronic conjugation has a quite sizable impact on the injection efficiency.

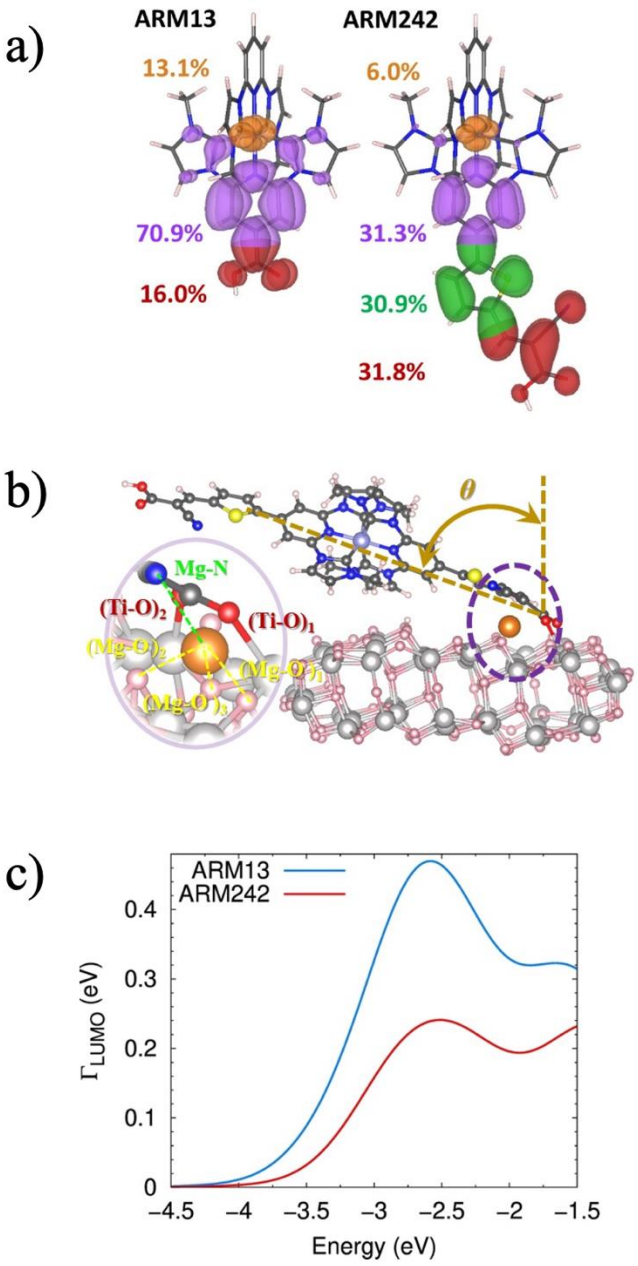

Figure 12. a) NTOs in **ARM13** and **ARM242** with the percentages of charge delocalization for each fragment (isovalue 0.02 a.u.); b) Optimized structure of **ARM12**@$Mg^{2+}TiO_2$ showing tilted angles (θ) between the normal surface vector and **ARM12**; c) Probability distribution Γ(ε) for electron injection from the LUMO of **ARM13** (blue) and **ARM242** (red) dyes to the TiO_2-Mg^{2+} states within the energy region of the TiO_2 CB edge. Data from ref. 4

By combining, however, the remarkable absorption red-shift in the broadening of the absorption domain, we obtained for the **C1**+**ARM12** co-sensitization a photocurrent of 9 mA/cm^2 and an average PCE of 2% that represents the best efficiency ever reported for a n-type sensitization by Fe(II) dyes.[4]

Conclusions and perspectives

In this account we demonstrate that iron-sensitized solar cells (FeSSCs) have now to be considered as potential earth-abundant metal-based alternatives to their noble metal containing analogues. This has been made possible by our efforts to combine a quantum chemical simulation assisted rational molecular design of Fe(II)NHC sensitizers, with an accurate experimental characterization of the interfacial electron transfer and recombination processes, allowing for electrolyte and device optimization. This synergic approach allowed to boost the cell efficiency from 0.13% and 0.41 mA.cm^{-2} in the very first attempts with an homoleptic sensitizer up to 2% (multiplied by a factor of 15) associated with the production of a 9 mA.cm^{-2} photocurrent (multiplied by a factor of 22) never reached yet in a FeSSC using tailor-made heteroleptic sensitizer photoanodes and electrolytes.

However, while being outstanding in the framework of iron-sensitizers solar cells, these performances are not yet sufficient to beat the ruthenium gold standard and improvements are necessary. Two main axes of progress can be identified. The Voc that until now peaks at about 0.45 V is hampering the production of higher photocurrents, it could be increased by a judicious chose of additives to play with the Fermi level of the semiconductor. New sensitizer designs need to be imagined especially those with extended absorption domains. In this context, the recently developed homo inversion concept that consists in increasing the energy of ligand π-orbitals via an increase of delocalization is a promising route to reach this goal. Preventing the

bending of the sensitizer on the TiO_2 surface should be also investigated by designing various multifunctional anchoring sites in order to promote a rigidification at the dye/SC interface.

To conclude, we think that this account will serve as a foundation for future works in the area of iron-based sensitization for electron transfer that, while in its infancy can be considered as realistic and opens a playground for searchers involved in the course for the transition towards cheaper and ecofriendly solar devices.

Acknowledgments

The authors would like to warmly thank all the collaborators from their respective groups for their dedicated experimental and theoretical work. P.C.G. is grateful to French Agence Nationale de Recherche (ANR-16-CE07-0013-02), Lorraine Université d'Excellence (IMPACT N4S) and the European Regional Development Funds (Programme opérationnel FEDER-FSE Lorraine et Massif des Vosges 2014-2020/"Fire Light" project: "Photo-bio-active molecules and nanoparticles" for financial supports.

Biographies

Mariachiara Pastore got her PhD in theoretical chemistry at the University of Ferrara (Italy) in 2009. She joined the CNRS as senior researcher in 2015 in the Laboratoire de Physique et Chimie Théoriques (LPCT) in Nancy (France). Her research interests span from the development and application of highly correlated ab initio methods (multireference perturbation theories) and hybrid density functional theory/wavefunction-based methods to the study of excited states in small and medium size molecules, to the characterization of the optical and charge separation properties in molecule/semiconductor interfaces for solar energy and solar fuels applications.

Stefano Caramori is professor of Inorganic Chemistry at the University of Ferrara, where he has been teaching Inorganic Chemistry and Photoelectrochemistry since 2012. His main research interests are related to light matter/interactions and electron transfer reaction in heterogeneous systems with applicationsin the fields of solar energy conversion, metal electrode, semiconductor sensitization, redox shuttles and photocatalysis for environmental remediation.

Philippe C. Gros received his PhD from the University Claude Bernard in Lyon (France) in 1992. After post-doctoral research with CNRS & industry, he joined the CNRS in 1994 as a Research associate. He is presently first-class CNRS Research Director in the Laboratoire Lorrain de Chimie Moléculaire (L2CM) in Nancy (France) for which he served as the director (2018–2021). His research interests cover synthetic organometallic methodologies, design of tailor-made ligands and their transition metal complexes (Fe, Ru, Co) with applications in various fields such as solar energy conversion and cancer diagnostic and treatment.

References

(1) Duchanois, T.; Etienne, T.; Cebrián, C.; Liu, L.; Monari, A.; Beley, M.; Assfeld, X.; Haacke, S.; Gros, P. C. An Iron-Based Photosensitizer with Extended Excited-State Lifetime: Photophysical and Photovoltaic Properties. *Eur. J. Inorg. Chem.* **2015**, *2015*, 2469–2477.

(2) Reddy Marri, A.; Marchini, E.; Cabanes, V. D.; Argazzi, R.; Pastore, M.; Caramori, S.; Gros, P. C. Record Power Conversion Efficiencies for Iron(II)-NHC-Sensitized DSSCs from Rational Molecular Engineering and Electrolyte Optimization. *J. Mater. Chem. A* **2021**, *9*, 3540–3554.

(3) Marri, A. R.; Marchini, E.; Cabanes, V. D.; Argazzi, R.; Pastore, M.; Caramori, S.; Bignozzi, C. A.; Gros, P. C. A Series of Iron(II)-NHC Sensitizers with Remarkable Power Conversion Efficiency in Photoelectrochemical Cells**. *Chem. – Eur. J.* **2021**, *27*, 16260–16269.

(4) Reddy-Marri, A.; Marchini, E.; Cabanes, V. D.; Argazzi, R.; Pastore, M.; Caramori, S.; Gros, P. C. Panchromatic Light Harvesting and Record Power Conversion Efficiency for Carboxylic/Cyanoacrylic Fe(II) NHC Co-Sensitized FeSSCs. *Chem. Sci.* **2023**, *14*, 4288–4301.

(5) Freitag, M.; Boschloo, G. The Revival of Dye-Sensitized Solar Cells. *Curr. Opin. Electrochem.* **2017**, *2*, 111–119.

(6) Freitag, M.; Teuscher, J.; Saygili, Y.; Zhang, X.; Giordano, F.; Liska, P.; Hua, J.; Zakeeruddin, S. M.; Moser, J.-E.; Grätzel, M.; Hagfeldt, A. Dye-Sensitized Solar Cells for Efficient Power Generation under Ambient Lighting. *Nat. Photonics* **2017**, *11*, 372–378.
(7) Cao, Y.; Liu, Y.; Zakeeruddin, S. M.; Hagfeldt, A.; Grätzel, M. Direct Contact of Selective Charge Extraction Layers Enables High-Efficiency Molecular Photovoltaics. *Joule* **2018**, *2*, 1108–1117.
(8) Michaels, H.; Rinderle, M.; Benesperi, I.; Freitag, R.; Gagliardi, A.; Freitag, M. Emerging Indoor Photovoltaics for Self-Powered and Self-Aware IoT towards Sustainable Energy Management. *Chem. Sci.* **2023**, *14*, 5350–5360.
(9) Hagfeldt, A.; Boschloo, G.; Sun, L.; Kloo, L.; Pettersson, H. Dye-Sensitized Solar Cells. *Chem. Rev.* **2010**, *110*, 6595–6663.
(10) Diez-Cabanes, V.; Fantacci, S.; Pastore, M. First-Principles Modeling of Dye-Sensitized Solar Cells: From the Optical Properties of Standalone Dyes to the Charge Separation at Dye/TiO2 Interfaces. In *Theoretical and Computational Photochemistry*; Elsevier, 2023; pp 215–245.
(11) Pastore, M.; De Angelis, F. Modeling Materials and Processes in Dye-Sensitized Solar Cells: Understanding the Mechanism, Improving the Efficiency. In *Multiscale Modelling of Organic and Hybrid Photovoltaics*; Beljonne, D., Cornil, J., Eds.; Topics in Current Chemistry; Springer Berlin Heidelberg: Berlin, Heidelberg, 2013; Vol. 352, pp 151–236.
(12) Sakurai, J. J.; Napolitano, J. *Modern Quantum Mechanics:*, 2nd ed.; Cambridge University Press, 2017.
(13) Balzani, V.; Scandola, F. *Supramolecular Photochemistry*; Ellis Horwood series in physical chemistry; Ellis Horwood, 1991.
(14) Sharma, K.; Sharma, V.; Sharma, S. S. Dye-Sensitized Solar Cells: Fundamentals and Current Status. *Nanoscale Res. Lett.* **2018**, *13*, 381.
(15) Kishore Kumar, D.; Kříž, J.; Bennett, N.; Chen, B.; Upadhayaya, H.; Reddy, K. R.; Sadhu, V. Functionalized Metal Oxide Nanoparticles for Efficient Dye-Sensitized Solar Cells (DSSCs): A Review. *Mater. Sci. Energy Technol.* **2020**, *3*, 472–481.
(16) Ye, M.; Wen, X.; Wang, M.; Iocozzia, J.; Zhang, N.; Lin, C.; Lin, Z. Recent Advances in Dye-Sensitized Solar Cells: From Photoanodes, Sensitizers and Electrolytes to Counter Electrodes. *Mater. Today* **2015**, *18*, 155–162.
(17) Shaikh, J. S.; Shaikh, N. S.; Mali, S. S.; Patil, J. V.; Pawar, K. K.; Kanjanaboos, P.; Hong, C. K.; Kim, J. H.; Patil, P. S. Nanoarchitectures in Dye-Sensitized Solar Cells: Metal Oxides, Oxide Perovskites and Carbon-Based Materials. *Nanoscale* **2018**, *10*, 4987–5034.
(18) Parisi, M. L.; Dessì, A.; Zani, L.; Maranghi, S.; Mohammadpourasl, S.; Calamante, M.; Mordini, A.; Basosi, R.; Reginato, G.; Sinicropi, A. Combined LCA and Green Metrics Approach for the Sustainability Assessment of an Organic Dye Synthesis on Lab Scale. *Front. Chem.* **2020**, *8*, 214.
(19) Wang, X.; Zhao, B.; Kan, W.; Xie, Y.; Pan, K. Review on Low-Cost Counter Electrode Materials for Dye-Sensitized Solar Cells: Effective Strategy to Improve Photovoltaic Performance. *Adv. Mater. Interfaces* **2022**, *9*, 2101229.
(20) Schoden, F.; Schnatmann, A. K.; Blachowicz, T.; Manz-Schumacher, H.; Schwenzfeier-Hellkamp, E. Circular Design Principles Applied on Dye-Sensitized Solar Cells. *Sustainability* **2022**, *14* (22), 15280.
(21) Spinelli, G.; Freitag, M.; Benesperi, I. What Is Necessary to Fill the Technological Gap to Design Sustainable Dye-Sensitized Solar Cells? *Sustain. Energy Fuels* **2023**, *7*, 916–927.
(22) Grätzel, M. Photoelectrochemical Cells. *Nature* **2001**, *414*, 338–344.

(23) Tomar, N.; Agrawal, A.; Dhaka, V. S.; Surolia, P. K. Ruthenium Complexes Based Dye Sensitized Solar Cells: Fundamentals and Research Trends. *Sol. Energy* **2020**, *207*, 59–76.
(24) De Angelis, F.; Fantacci, S.; Selloni, A.; Nazeeruddin, M. K.; Grätzel, M. First-Principles Modeling of the Adsorption Geometry and Electronic Structure of Ru(II) Dyes on Extended TiO_2 Substrates for Dye-Sensitized Solar Cell Applications. *J. Phys. Chem. C* **2010**, *114*, 6054–6061.
(25) Pastore, M.; Fantacci, S.; De Angelis, F. Modeling Excited States and Alignment of Energy Levels in Dye-Sensitized Solar Cells: Successes, Failures, and Challenges. *J. Phys. Chem. C* **2013**, *117*, 3685–3700.
(26) Pastore, M.; Selloni, A.; Fantacci, S.; De Angelis, F. Electronic and Optical Properties of Dye-Sensitized TiO2 Interfaces. In *First Principles Approaches to Spectroscopic Properties of Complex Materials*; Di Valentin, C., Botti, S., Cococcioni, M., Eds.; Topics in Current Chemistry; Springer Berlin Heidelberg: Berlin, Heidelberg, 2014; Vol. 347, pp 1–45.
(27) Koops, S. E.; O'Regan, B. C.; Barnes, P. R. F.; Durrant, J. R. Parameters Influencing the Efficiency of Electron Injection in Dye-Sensitized Solar Cells. *J. Am. Chem. Soc.* **2009**, *131*, 4808–4818.
(28) Durrant, J. R.; Haque, S. A.; Palomares, E. Towards Optimisation of Electron Transfer Processes in Dye Sensitised Solar Cells. *Coord. Chem. Rev.* **2004**, *248*, 1247–1257.
(29) Listorti, A.; Creager, C.; Sommeling, P.; Kroon, J.; Palomares, E.; Fornelli, A.; Breen, B.; Barnes, P. R. F.; Durrant, J. R.; Law, C.; O'Regan, B. The Mechanism behind the Beneficial Effect of Light Soaking on Injection Efficiency and Photocurrent in Dye Sensitized Solar Cells. *Energy Environ. Sci.* **2011**, *4* (9), 3494–3501.
(30) Listorti, A.; O'Regan, B.; Durrant, J. R. Electron Transfer Dynamics in Dye-Sensitized Solar Cells. *Chem. Mater.* **2011**, *23* (15), 3381–3399.
(31) Housecroft, C. E.; Constable, E. C. The Emergence of Copper(I)-Based Dye Sensitized Solar Cells. *Chem. Soc. Rev.* **2015**, *44*, 8386–8398.
(32) Sandroni, M.; Pellegrin, Y.; Odobel, F. Heteroleptic Bis-Diimine Copper(I) Complexes for Applications in Solar Energy Conversion. *Comptes Rendus Chim.* **2016**, *19*), 79–93.
(33) Mishra, A.; Fischer, M. K. R.; Bäuerle, P. Metal-Free Organic Dyes for Dye-Sensitized Solar Cells: From Structure: Property Relationships to Design Rules. *Angew. Chem. Int. Ed.* **2009**, *48*, 2474–2499.
(34) Zeng, W.; Cao, Y.; Bai, Y.; Wang, Y.; Shi, Y.; Zhang, M.; Wang, F.; Pan, C.; Wang, P. Efficient Dye-Sensitized Solar Cells with an Organic Photosensitizer Featuring Orderly Conjugated Ethylenedioxythiophene and Dithienosilole Blocks. *Chem. Mater.* **2010**, *22*, 1915–1925.
(35) Zhang, L.; Yang, X.; Wang, W.; Gurzadyan, G. G.; Li, J.; Li, X.; An, J.; Yu, Z.; Wang, H.; Cai, B.; Hagfeldt, A.; Sun, L. 13.6% Efficient Organic Dye-Sensitized Solar Cells by Minimizing Energy Losses of the Excited State. *ACS Energy Lett.* **2019**, *4*, 943–951.
(36) Ferrere, S. New Photosensitizers Based upon $[Fe(L)_2(CN)_2]$ and $[Fe(L)_3]$ (L = Substituted 2,2'-Bipyridine): Yields for the Photosensitization of TiO_2 and Effects on the Band Selectivity. *Chem. Mater.* **2000**, *12*, 1083–1089.
(37) Ferrere, S.; Gregg, B. A. Photosensitization of TiO_2 by $[Fe^{II}(2,2'\text{-Bipyridine-4,4'-Dicarboxylic Acid})_2(CN)_2]$: Band Selective Electron Injection from Ultra-Short-Lived Excited States. *J. Am. Chem. Soc.* **1998**, *120*, 843–844.
(38) Monat, J. E.; McCusker, J. K. Femtosecond Excited-State Dynamics of an Iron(II) Polypyridyl Solar Cell Sensitizer Model. *J. Am. Chem. Soc.* **2000**, *122*, 4092–4097.

(39) Auböck, G.; Chergui, M. Sub-50-Fs Photoinduced Spin Crossover in [Fe(Bpy)3]2+. *Nat. Chem.* **2015**, *7*, 629–633.
(40) Smeigh, A. L.; Creelman, M.; Mathies, R. A.; McCusker, J. K. Femtosecond Time-Resolved Optical and Raman Spectroscopy of Photoinduced Spin Crossover: Temporal Resolution of Low-to-High Spin Optical Switching. *J. Am. Chem. Soc.* **2008**, *130*, 14105–14107.
(41) Cammarata, M.; Bertoni, R.; Lorenc, M.; Cailleau, H.; Di Matteo, S.; Mauriac, C.; Matar, S. F.; Lemke, H.; Chollet, M.; Ravy, S.; Laulhé, C.; Létard, J.-F.; Collet, E. Sequential Activation of Molecular Breathing and Bending during Spin-Crossover Photoswitching Revealed by Femtosecond Optical and X-Ray Absorption Spectroscopy. *Phys. Rev. Lett.* **2014**, *113*,227402.
(42) Dierks, P.; Päpcke, A.; Bokareva, O. S.; Altenburger, B.; Reuter, T.; Heinze, K.; Kühn, O.; Lochbrunner, S.; Bauer, M. Ground- and Excited-State Properties of Iron(II) Complexes Linked to Organic Chromophores. *Inorg. Chem.* **2020**, *59*, 14746–14761.
(43) Francés-Monerris, A.; Gros, P. C.; Assfeld, X.; Monari, A.; Pastore, M. Toward Luminescent Iron Complexes: Unravelling the Photophysics by Computing Potential Energy Surfaces. *ChemPhotoChem* **2019**, *3*, 666–683.
(44) Liu, Y.; Harlang, T.; Canton, S. E.; Chábera, P.; Suárez-Alcántara, K.; Fleckhaus, A.; Vithanage, D. A.; Göransson, E.; Corani, A.; Lomoth, R.; Sundström, V.; Wärnmark, K. Towards Longer-Lived Metal-to-Ligand Charge Transfer States of Iron(II) Complexes: An N-Heterocyclic Carbene Approach. *Chem. Commun.* **2013**, *49*, 6412–6414.
(45) Duchanois, T.; Liu, L.; Pastore, M.; Monari, A.; Cebrián, C.; Trolez, Y.; Darari, M.; Magra, K.; Francés-Monerris, A.; Domenichini, E.; Beley, M.; Assfeld, X.; Haacke, S.; Gros, P. NHC-Based Iron Sensitizers for DSSCs. *Inorganics* **2018**, *6*, 63.
(46) Liu, Y.; Persson, P.; Sundström, V.; Wärnmark, K. Fe *N* -Heterocyclic Carbene Complexes as Promising Photosensitizers. *Acc. Chem. Res.* **2016**, *49*, 1477–1485.
(47) Liu, L.; Duchanois, T.; Etienne, T.; Monari, A.; Beley, M.; Assfeld, X.; Haacke, S.; Gros, P. C. A New Record Excited State ^{3} MLCT Lifetime for Metalorganic Iron(II) Complexes. *Phys Chem Chem Phys* **2016**, *18*, 12550–12556.
(48) Darari, M.; Domenichini, E.; Francés-Monerris, A.; Cebrián, C.; Magra, K.; Beley, M.; Pastore, M.; Monari, A.; Assfeld, X.; Haacke, S.; Gros, P. C. Iron(II) Complexes with Diazinyl-NHC Ligands: Impact of π-Deficiency of the Azine Core on Photophysical Properties. *Dalton Trans.* **2019**, *48*, 10915–10926.
(49) Magra, K.; Darari, M.; Domenichini, E.; Francés-Monerris, A.; Cebrián, C.; Beley, M.; Pastore, M.; Monari, A.; Assfeld, X.; Haacke, S.; Gros, P. C. Photophysical Investigation of Iron(II) Complexes Bearing Bidentate Annulated Isomeric Pyridine-NHC Ligands. *J. Phys. Chem. C* **2020**, *124*, 18379–18389.
(50) Magra, K.; Domenichini, E.; Francés-Monerris, A.; Cebrián, C.; Beley, M.; Darari, M.; Pastore, M.; Monari, A.; Assfeld, X.; Haacke, S.; Gros, P. C. Impact of the *Fac* / *Mer* Isomerism on the Excited-State Dynamics of Pyridyl-Carbene Fe(II) Complexes. *Inorg. Chem.* **2019**, *58*, 5069–5081.
(51) Romero, N. A.; Nicewicz, D. A. Organic Photoredox Catalysis. *Chem. Rev.* **2016**, *116*, 10075–10166.
(52) Crisenza, G. E. M.; Melchiorre, P. Chemistry Glows Green with Photoredox Catalysis. *Nat. Commun.* **2020**, *11*, 803.

(53) Pastore, M.; Duchanois, T.; Liu, L.; Monari, A.; Assfeld, X.; Haacke, S.; Gros, P. C. Interfacial Charge Separation and Photovoltaic Efficiency in Fe(II)–Carbene Sensitized Solar Cells. *Phys Chem Chem Phys* **2016**, *18*, 28069–28081.
(54) Lindh, L.; Gordivska, O.; Persson, S.; Michaels, H.; Fan, H.; Chábera, P.; Rosemann, N. W.; Gupta, A. K.; Benesperi, I.; Uhlig, J.; Prakash, O.; Sheibani, E.; Kjaer, K. S.; Boschloo, G.; Yartsev, A.; Freitag, M.; Lomoth, R.; Persson, P.; Wärnmark, K. Dye-Sensitized Solar Cells Based on Fe N-Heterocyclic Carbene Photosensitizers with Improved Rod-like Push-Pull Functionality. *Chem. Sci.* **2021**, *12*, 16035–16053.
(55) Fredin, L. A.; Pápai, M.; Rozsályi, E.; Vankó, G.; Wärnmark, K.; Sundström, V.; Persson, P. Exceptional Excited-State Lifetime of an Iron(II)– *N* -Heterocyclic Carbene Complex Explained. *J. Phys. Chem. Lett.* **2014**, *5*, 2066–2071.
(56) Becker, M.; Wyss, V.; Housecroft, C. E.; Constable, E. C. The Influence of Alkyl Chains on the Performance of DSCs Employing Iron(II) N-Heterocyclic Carbene Sensitizers. *Dalton Trans.* **2021**, *50*, 16961–16969.
(57) Marchini, E.; Darari, M.; Lazzarin, L.; Boaretto, R.; Argazzi, R.; Bignozzi, C. A.; Gros, P. C.; Caramori, S. Recombination and Regeneration Dynamics in FeNHC(II)-Sensitized Solar Cells. *Chem. Commun.* **2020**, *56*, 543–546.
(58) Karpacheva, M.; Wyss, V.; Housecroft, C. E.; Constable, E. C. There Is a Future for N-Heterocyclic Carbene Iron(II) Dyes in Dye-Sensitized Solar Cells: Improving Performance through Changes in the Electrolyte. *Materials* **2019**, *12*, 4181.
(59) Becker, M.; Housecroft, C. E.; Constable, E. C. Electrolyte Tuning in Iron(II)-Based Dye-Sensitized Solar Cells: Different Ionic Liquids and I2 Concentrations. *Materials* **2021**, *14*, 3053.
(60) Harlang, T. C. B.; Liu, Y.; Gordivska, O.; Fredin, L. A.; Ponseca, C. S.; Huang, P.; Chábera, P.; Kjaer, K. S.; Mateos, H.; Uhlig, J.; Lomoth, R.; Wallenberg, R.; Styring, S.; Persson, P.; Sundström, V.; Wärnmark, K. Iron Sensitizer Converts Light to Electrons with 92% Yield. *Nat. Chem.* **2015**, *7*, 883–889.
(61) Boschloo, G.; Häggman, L.; Hagfeldt, A. Quantification of the Effect of 4- *Tert* -Butylpyridine Addition to I^-/I_3^- Redox Electrolytes in Dye-Sensitized Nanostructured TiO_2 Solar Cells. *J. Phys. Chem. B* **2006**, *110*, 13144–13150.
(62) Marchini, E.; Darari, M.; Lazzarin, L.; Boaretto, R.; Argazzi, R.; Bignozzi, C. A.; Gros, P. C.; Caramori, S. Recombination and Regeneration Dynamics in FeNHC(II)-Sensitized Solar Cells. *Chem. Commun.* **2020**, *56*, 543–546.
(63) Koops, S. E.; O'Regan, B. C.; Barnes, P. R. F.; Durrant, J. R. Parameters Influencing the Efficiency of Electron Injection in Dye-Sensitized Solar Cells. *J. Am. Chem. Soc.* **2009**, *131*, 4808–4818.
(64) Agrawal, S.; Leijtens, T.; Ronca, E.; Pastore, M.; Snaith, H.; De Angelis, F. Modeling the Effect of Ionic Additives on the Optical and Electronic Properties of a Dye-Sensitized TiO2 Heterointerface: Absorption, Charge Injection and Aggregation. *J. Mater. Chem. A* **2013**, *1* (46), 14675–14685.
(65) Karpacheva, M.; Housecroft, C. E.; Constable, E. C. Electrolyte Tuning in Dye-Sensitized Solar Cells with *N* -Heterocyclic Carbene (NHC) Iron(II) Sensitizers. *Beilstein J. Nanotechnol.* **2018**, *9*, 3069–3078.
(66) Zhang, L.; Cole, J. M. Anchoring Groups for Dye-Sensitized Solar Cells. *ACS Appl. Mater. Interfaces* **2015**, *7*, 3427–3455.
(67) Cole, J. M.; Blood-Forsythe, M. A.; Lin, T.-C.; Pattison, P.; Gong, Y.; Vázquez-Mayagoitia, Á.; Waddell, P. G.; Zhang, L.; Koumura, N.; Mori, S. Discovery of S···C≡N

Intramolecular Bonding in a Thiophenylcyanoacrylate-Based Dye: Realizing Charge Transfer Pathways and Dye···TiO_2 Anchoring Characteristics for Dye-Sensitized Solar Cells. *ACS Appl. Mater. Interfaces* **2017**, *9*, 25952–25961.